Dynamic Response of a Rotor Supported on a Floating Ring Bearing

Julio Naranjo and Chris Holt,
Graduate Research Assistants
Luis San Andrés, Professor
Mechanical Engineering Department
Texas A&M University
College Station, TX 77843-3123

ABSTRACT

Turbochargers (*TC*) increase the power output and efficiency of internal combustion automotive engines. Conventional *TC* rotors are usually supported on floating ring journal bearings (*FRBs*) comprising two thin lubricated films in series. *FRBs* offer lower power losses, damping characteristics, and also cooler operating conditions than simple hydrodynamic journal bearings. Although *TC* on *FRBs* exhibit sub synchronous rotor whirl in most of their operating range, they often reach stable limit cycles, thus becoming cost-effective solutions in a competitive market. Measurements of the dynamic response to imbalance on a small test rotor supported on a floating ring bearing are presented. Threshold speeds of instability, sub critical bifurcations, amplitudes of limit cycles, ranges of whirl frequencies as a function of bearing load, rotor imbalances, feed pressures and rotor speeds were characterized from the experiments. The rotor-*FRB* nonlinear response shows two self-excited sub synchronous vibration components related to the hydrodynamic instability of the inner and outer films of the *FRB*. A linear rotordynamics model predicts poorly the onset speed of the instability and offers no insight in estimating the limit cycle amplitudes of rotor motion. Localized absence of sub synchronous vibration components was observed within specific rotor speed ranges for high feed pressures emulating large loads. The dynamic response of the rotor supported on a semi-*FRB* was also tested and found to be less favorable due to high levels of vibration induced by air entrainment into the outer film.

Keywords: Fluid film bearings, rotordynamic instability, modeling and experiments

INTRODUCTION

Floating Ring Bearings (*FRBs*) are typically used as support elements in turbochargers for automotive applications. *FRBs*, as depicted in Figure 1, comprise inner and outer thin films in series. A supply plenum delivers engine lubricant to the outer film, and holes machined on the floating ring permit the passage of oil towards the inner film lands. Deep grooves on the ring divide each film into two equal film lands and ensure a uniform feed pressure around the ring circumference. The ring spins at a fraction of the rotor speed, thereby reducing the shear drag losses [1, 2], but increasing the resistance to maintain a uniform fluid flow towards the inner film lands. The journal and ring vibrate due to aerodynamic loads, rotor imbalance, or transmitted forces and noise from the engine

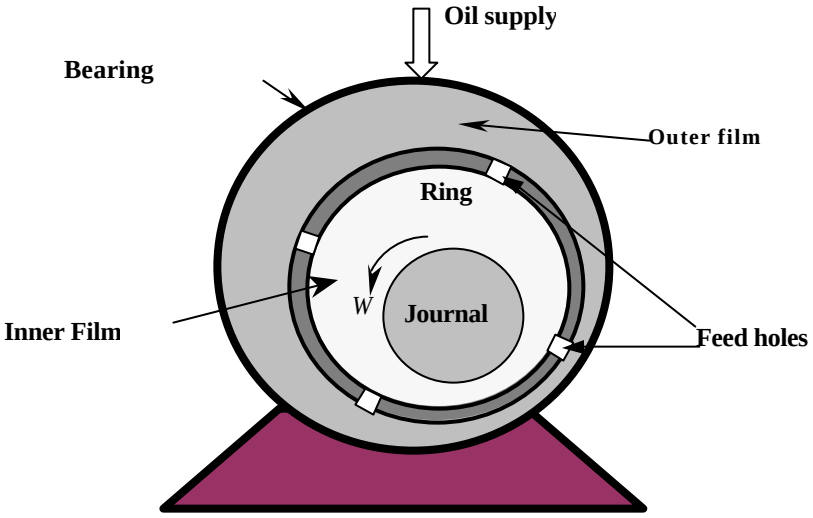

Figure 1. Schematic representation of a floating ring bearing.

frame. *FRBs* allow operation at cooler conditions and provide enhanced energy dissipation of rotor vibrational energy than with plain cylindrical journal bearings [2]. In some automotive applications, a locking pin in the ring prevents its rotation and enables semi-floating ring bearing (*SFRB*) operation, similar to a squeeze film damper.

FRBs thus offer the advantages of inherent damping, simplicity in design, low cost production and tolerance of engine oil as a lubricant. However, *FRBs* and *SFRBs* are prone to show sub synchronous whirl as with plain journal bearings, and in most cases, undergo large vibration amplitudes within the bearing clearances [3,4]. Sub synchronous vibration induces fatigue of the rotating parts and reduces considerably the life of the rotor-bearing system. Despite this behavior, *FRBs* often reach stable limit cycles [5, 6, 7] and become cost effective solutions in a competitive market [8]. Figure 2 shows the acceleration spectrum recorded on the casing of a commercial turbocharger at a rotor speed of 80,000 rpm (1,333 Hz). Note the large sub synchronous vibration components at 444 Hz and 612 Hz, i.e. at 33% and 45% of shaft speed. No analytical model is yet available to properly predict the amplitude and frequencies of the recorded rotordynamic response [9].

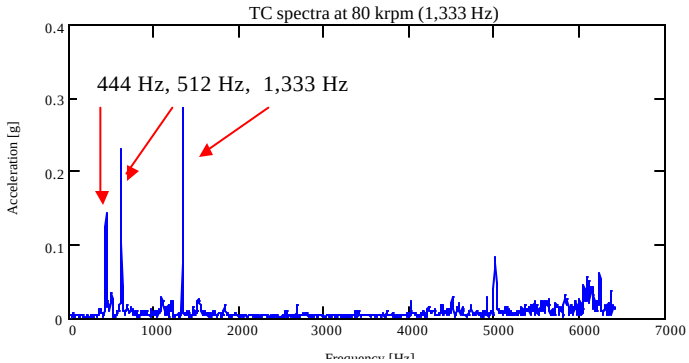

Figure 2. Acceleration spectrum on casing of turbocharger test rig at a rotor speed of 80,000 rpm (1,333 Hz).

The dynamics of *FRBs* are not yet well understood, and the effects of operating parameters such as pressure supply and oil temperature have received little attention. This paper reports detailed measurements of the dynamic response on a flexible rotor supported on a *FRB*. The experiments show the typical rotordynamic instabilities associated with plain

hydrodynamic bearings, and demonstrate the limited applicability of current (linear) analysis to predict the onset speed of instability and the ensuing sub synchronous dynamic response.

DESCRIPTION OF TEST RIG

A low speed (<10, 000 rpm) rotor-*FRB* test rig was constructed to display similar dynamic behavior as that expected in automotive turbochargers [10]. Figures 3 and 4 depict a schematic view of the apparatus and a detail of the floating ring bearing, respectively. A 1/10-HP DC electrical motor (1) drives the test rotor through a flexible coupling (2). The rotor consists of a slender shaft (11), 10 mm in diameter and 565 mm in length, and two heavy disks (6) weighing 0.80 kg each and press fitted in one end of the shaft. At the drive end, the rotor is mounted on two bronze bushings (3) with backing O-rings. A floating ring journal bearing, *FRB,*(5) also supports the rotor on the disks side. A mechanism (7) comprising four adjustable soft springs serves to align the shaft centerline and to offset the static load applied to the *FRB* by loosening or tightening bolts connected to the springs.

REFERENCES

1.- DRIVE MOTOR
2.- FLEXIBLE COUPLING
3.- BRONZE BUSHING
4.- DISPLACEMENT TRANSDUCERS
5.- **FLOATING RING BEARING HOUSING**
6.- DISKS
7.- SPRING ALIGNMENT MECHANISM
8.- DISPLACEMENT TRANSDUCERS
9.-RING
10.-JOURNAL
11.-SHAFT
12.-SUPPORT STRUCTURE (V-TYPE)

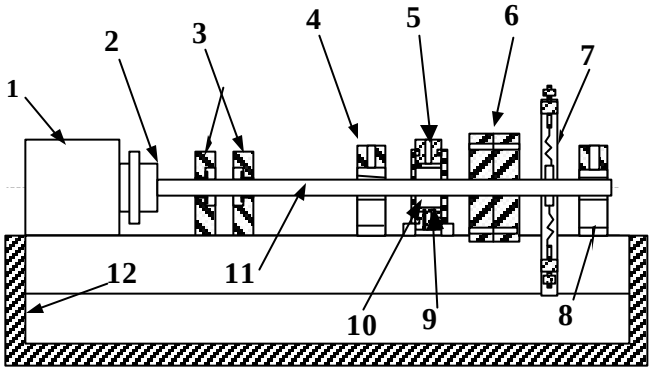

Figure 3. Schematic view of rotor-FRB test rig.

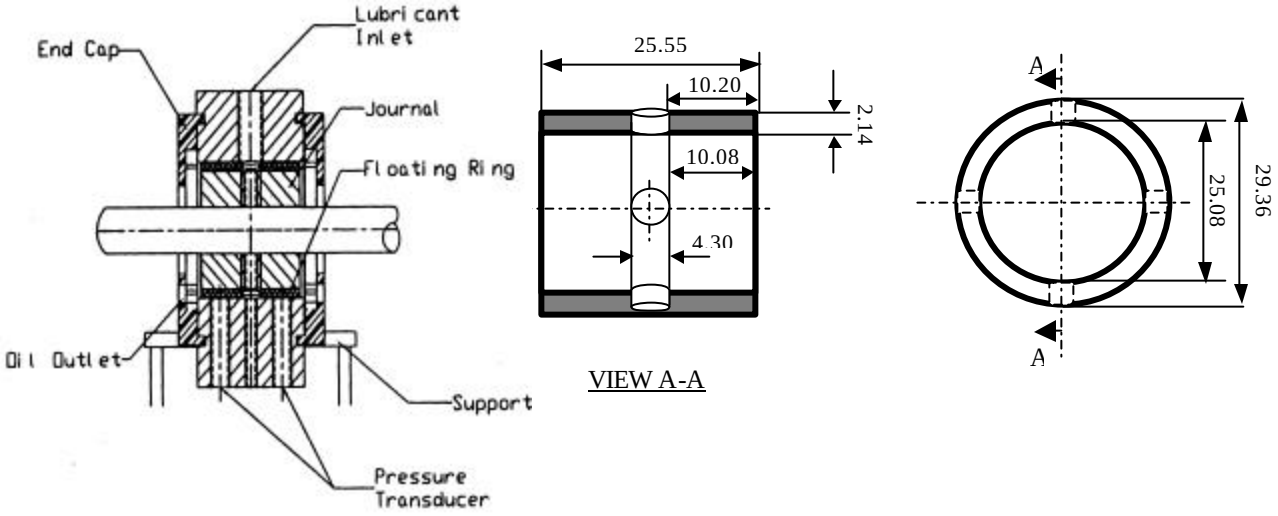

Figure 4. Detail of FRB assembly and floating ring dimensions (mm).

A variable speed pump supplies ISO VG 22 lubricant to the *FRB*. The oil density is 856 kg/m^3 with a measured viscosity equal to 33 and 27 centipoise at 25 °and 30 °C, respectively. An electric heater/chiller keeps the lubricant at the required temperature.

Three floating rings weighing 29-31 grams were manufactured to produce different film clearances. Figure 4 shows the nominal floating ring dimensions. The measured inner and outer film radial clearances for the three *FRB* configurations are:

nominal:	C_i=0.114 mm,	C_o=0.165 mm,	C_i/C_o=0.69
n+	0.152 mm,	0.190 mm,	0.80
n-	0.114 mm,	0.152 mm,	0.75,

with a ± 12.7 μm uncertainty.

Six eddy current displacement transducers recorded the amplitude of vibration of the shaft and the floating ring at two radial planes (vertical and horizontal). Two keyphasors measured the rotational speeds of the ring and shaft. An electronic control allowed setting desired rotor speeds and rotor run-up (down) rates. A Bourdon type pressure gauge connected to the supply line displayed the feed pressure into the *FRB*, and a strain-gauge transducer installed at the bottom of the bearing housing measured the hydrodynamic pressure generated by the outer film. K-type thermocouples recorded the oil temperatures at the inlet and discharge ports of the *FRB*. The signal output of the displacement sensors, the pressure transducer, and the shaft and ring speeds were collected with a Data Acquisition Interface Unit, and then processed with a rotordynamics diagnostics software in a personal computer.

ROTORDYNAMIC ANALYSIS OF TEST ROTOR-FRB

Predictions to determine the steady state (equilibrium) performance of the test *FRB* were obtained from a simple analysis using the short length bearing model [11]. Specified conditions of external load, lubricant viscosity and journal speed render the ring (e_R) and journal (e_J) eccentricities and ring to shaft speed ratio (Ω_R/W_J). For the nominal clearance *FRB*, Figure 5 displays the predicted ring/journal speed ratio and the dimensionless journal displacement $(e/[C_i+C_o])$ under a static load of 2.85 N, corresponding to a feed pressure equal to 13.8 kPa (2 psi). As the rotor speed increases, the journal and ring move towards the bearing center, and the ring rotational speed varies from 38% to 47% of the rotor speed.

Stiffness and damping coefficients for the inner and outer films in the *FRB* were determined. References [9] and [12] detail the analytical methods and numerical procedure using MATHCAD worksheets.

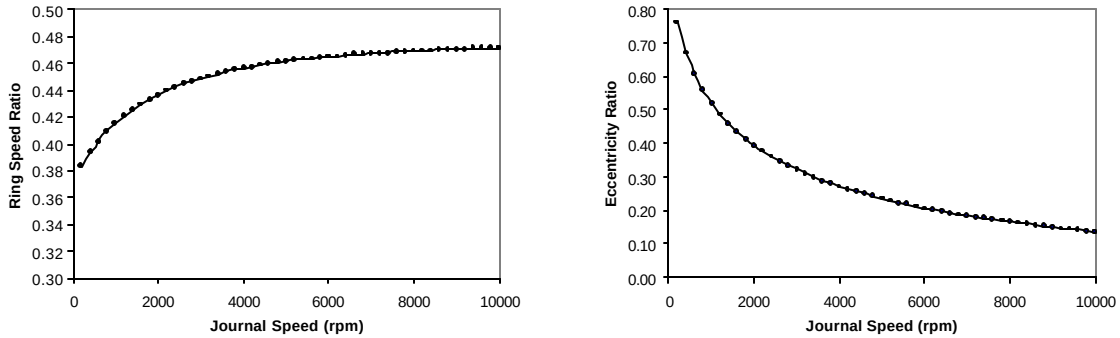

Figure 5. Predicted ring/shaft speed ratio and eccentricity ratio of *FRB*.

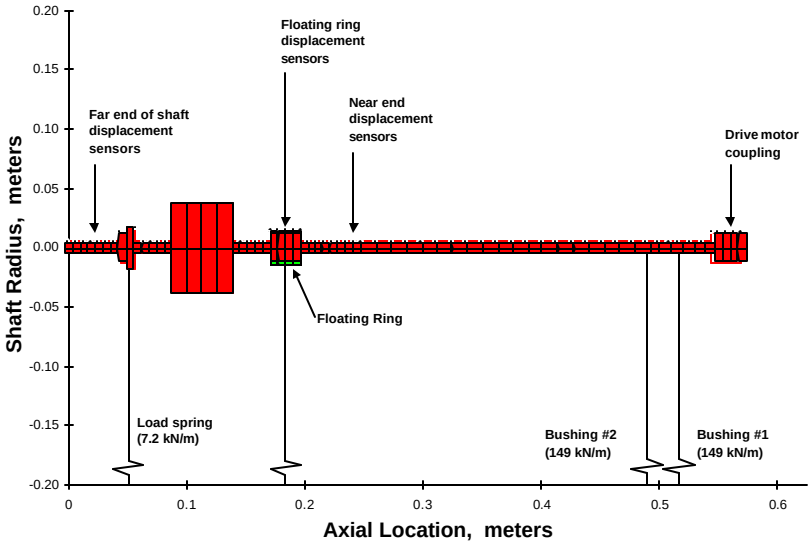

Figure 6. Structural FE model of rotor-*FRB* rig.

A rotordynamic analysis was next conducted to predict the eigenvalues (natural frequencies and damping ratios) and imbalance response of the rotor-*FRB* system. Figure 6 depicts a schematic view of the 70 station finite element model, with the floating ring as a minute secondary rotor. The measured bushing support and soft spring stiffnesses are 149 kN/m and 7.2 kN/m, respectively [9]. Predicted rotor-FRB natural frequencies agree well with experimental values from rap tests performed with a calibrated hammer and no rotor spinning, as shown below.

FRB	Natural frequency	Damping ratio	Prediction	Mode shape
Dry (w/o lubricant)	13 Hz	0.025	12.8 Hz	Rigid conical with node at drive end support
Wet (w/ lubricant)	46 Hz	0.112 (V), 0.121 (H)	46.1 Hz	Elastic with node near location of floating ring bearing

V: vertical and H: horizontal planes. Uncertainty in frequency +/- 1 Hz

Figure 7 shows the predicted damped natural frequencies for the rotor and active *FRB* versus rotor speed. In the graph, the letters *F* and *B* indicate forward and backward rotor modes, respectively. Lines of frequency synchronous with the shaft and ring rotational speeds are also shown. The model predicts an over damped first natural frequency (critical speed) at 875 rpm (14.6 Hz), corresponding to a conical rigid rotor mode. There

are three other natural frequencies at 4,820 rpm (3F), 6,450 rpm (2B) and 10,000 rpm, all associated with elastic rotor modes. A first instability (zero damping) system appears at a rotor speed of 4,120 rpm with a precessional frequency of ~18 Hz (1F), i.e. at a whirl frequency ratio equal to 0.27. A second instability should occur at a shaft speed of 7,100 rpm (118 Hz) with a whirl frequency of ~83 Hz, i.e. whirl ratio equal to 0.70. Relative to the ring rotational speed, only the first instability is sub synchronous.

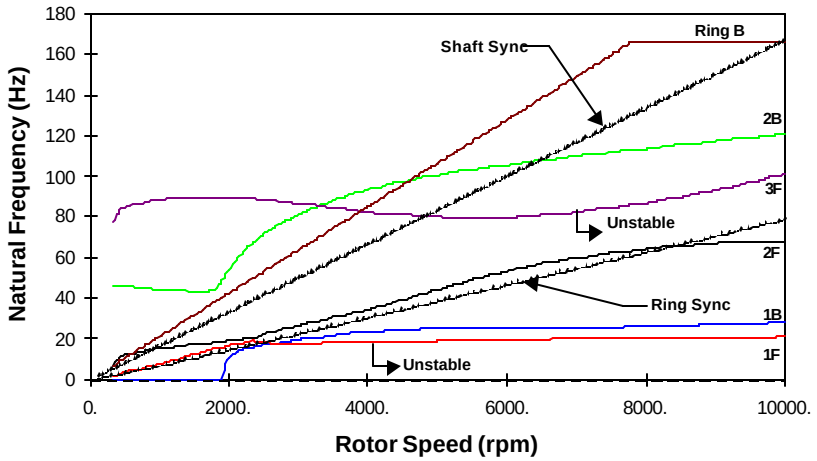

Figure 7. Damped natural frequency map for nominal clearance configuration (C_i=114.3 μm, Co=165.1 μm).

EXPERIMENTAL MEASUREMENTS

Run up (down) speed measurements of the dynamic response of the test-FRB rig were performed for the various ring configurations, supply pressures and imbalance conditions. Refer to Naranjo [9] for complete details on the experimental procedure and full set of measurements for the three *FRB* configurations. Figure 8 shows some of the experimental results for overall ring and shaft vibration amplitudes (Bode plots) as the rotor speed increases (decreases) to 8,000 rpm. The measurements correspond to the remnant imbalance condition in the rotor, and feed pressures equal to 13.8 kPa (2 psig) and 41.3 kPa (6 psig) emulating low and high static loads on the *FRB*. The rate of rotor acceleration (deceleration) was fixed at 3,000 rpm/min. The bottom graphs depict the ratio of synchronous amplitudes of motion to overall vibration, i.e. magnitudes near one show mostly a vibratory response synchronous with rotor speed, while low values indicate self-excited (rotordynamic) instabilities or motions not related to rotor imbalance.

Figure 9 shows the measured floating ring speed ratio versus rotor speed for the tests at the lowest feed pressure. Similar results were obtained for the feed pressure of 41.3 kPa and even with added imbalances located on the rotor disks. Predictions of the ring speed ratio, see Figure 5, are somewhat larger than the measured values prior to the onset speed of instability.

Figures 10 through 12 depict contour plots of the vibration spectra as the rotor decelerates from a top speed of 10,000 rpm. In these graphs, the horizontal axis represents the

frequency components of vibration and the vertical axis indicates the rotor speed in rpm/100. The colors in the graphs intend to show the severity of vibration, i.e. red color shows peak amplitudes of vibration. The slanted line in the graphs indicates synchronous vibration components. The measurements reported clearly evidence two rotordynamic instabilities (sub synchronous vibration) for most operating speeds.

DISCUSSION OF EXPERIMENTAL RESULTS

The measurements for the low feed pressure (emulating a low load condition on the *FRB*) evidence a threshold speed of instability at ~ 1600 rpm (~ 27 Hz) with a sub synchronous vibration component at a whirl frequency ratio of nearly ½. Note that the rotor speed when the first instability onsets is nearly twice the natural frequency of the dry-system (13 Hz), corresponding to the rigid rotor conical mode. As the rotor speed increases the sub synchronous whirl frequency tracks the rotor speed until it locks at approximately ~46 Hz, that is at the natural frequency of the lubricated (wet) system. When this event happens, the rotor speed is ~ 5,400 rpm (90 Hz), i.e. twice the value of the wet system natural frequency. At this speed, the rotor begins to vibrate violently with a second (locked) sub synchronous frequency at 18 Hz, i.e. approximately 20% of rotor speed. The 18 Hz and 46 Hz sub synchronous components of vibration are related to the hydrodynamic instability of the outer and inner films of the *FRB*, respectively[1].

The measurements with a larger feed pressure (larger static load) show the appearance of the ½ whirl frequency at the same threshold speed as in the low-pressure experiment. The rotor responses are very similar for both feed pressures up to a rotor speed of 5,400 rpm. Surprisingly, above this speed the rotor-*FRB* suddenly becomes stable with little vibratory response. However, as the rotor speed increases above 8,000 rpm, the two instabilities appear simultaneously albeit with somewhat different sub synchronous frequencies.

The Bode plots (Figure 8) show that the onset speed for the appearance or vanishing of sub synchronous vibrations (instabilities) depends on whether the rotor is accelerating (run up) or decelerating (run down). Sub synchronous vibration persists to speeds as low as 1,000 rpm, as the rotor decelerates, independent of the feed pressure or the rotor imbalance condition. The same behavior is noted for the high feed pressure test while suddenly becoming stable (or unstable) at rotor speeds 5,400 $\rightarrow$ 5,000 rpm. This behavior is indicative of sub critical bifurcations in a highly nonlinear rotor-bearing system.

The ring rotational speed undergoes a dramatic change at the onset speed of instability (~ 1,600 rpm), i.e. from 36 % of rotor speed to more than twice this value. As the rotor speed increases, the ring speed ratio slowly decreases. At 8,000 rpm, values of ring rotational speed are approximately 33% and 40 % of shaft speed for the tests at low and high feed pressures, respectively. Note that on the rotor run-down response, the ring speed ratio increases steadily until the shaft speed reaches 1,000 rpm; after which, a sudden decrease in ring speed occurs, bringing it back to the 33% and 40% values. The

[1] Measurements with a semi floating ring bearing only show one sub synchronous vibration component, typically at 46 Hz, and associated to the instability of the inner film [9].

sudden acceleration (deceleration) of the floating ring is probably due to the relative low mass moment of inertia of the rings used.

Note that the floating ring amplitude of motion is rather large once instability sets in (see top graphs in Figure 8). Recall that the diametrical clearance of the outer film equals 0.330 mm (13 mils). Figure 12 shows the contour spectra for an experiment with an added imbalance of 6 grams inserted at a radius of 30 mm in one of the rotor disks. The overall response is similar to that shown in Figure 10 for the remnant imbalance condition. However, the results in Figure 12 do show a significant synchronous vibration component. No evidence of rotor imbalance aiding to suppress the instabilities was ever observed in the experiments.

CONCLUSIONS

Measurements of the dynamic response of a test rotor supported on a floating ring bearing *(FRB)* are presented. The test rig emulates at low rotor speeds the dynamic conditions typically found in high speed turbochargers for automotive applications. The experimental results show that the rotor-*FRB* system reaches limit cycles within the bearing clearance. However, the rotor dynamic motion evidences two self-excited sub synchronous vibrations (instabilities) for most of the operating speed range. The first sub synchronous motion, due to the hydrodynamic instability of the inner film, appears at a relatively low rotor speed (1,560 rpm [26 Hz]) with a whirl ratio of ½, and follows the rotor speed until it locks at a frequency coinciding with the second natural frequency (46 Hz) of the rotor-*FRB* system. At a higher rotor speed, a second sub synchronous motion onsets and locks at a lower frequency (13 Hz), which also corresponds to the first natural frequency of the system. This second whirl is due to the hydrodynamic instability of the outer film in the *FRB*.

Under specific conditions of supply pressure (applied load), both rotor dynamic instabilities disappear within a narrow speed range. Furthermore, the experiments also reveal sub critical bifurcations typical of highly non linear dynamic systems.

Experiments with a semi floating ring configuration were also performed and not reported for brevity, see [9]. The measurements showed a less favorable rotordynamic response since the outer film collapsed as air entrained and formed a bubbly mixture.

The linear rotordynamic analysis offers no insight to realize the reported measurements, although it predicts well the system natural frequencies. The analysis[2] does predict two rotor-*FRB* instabilities, yet their onset and whirl frequency are not compatible with the measurements. A nonlinear analysis of the *FRB*s coupled to the rotor dynamics is thus urgently needed to advance the state of the art.

[2] DeBoer [12] recently advances an improved mo del able to predict all (two or more) threshold speeds of instability in rotors supported on floating ring bearings.

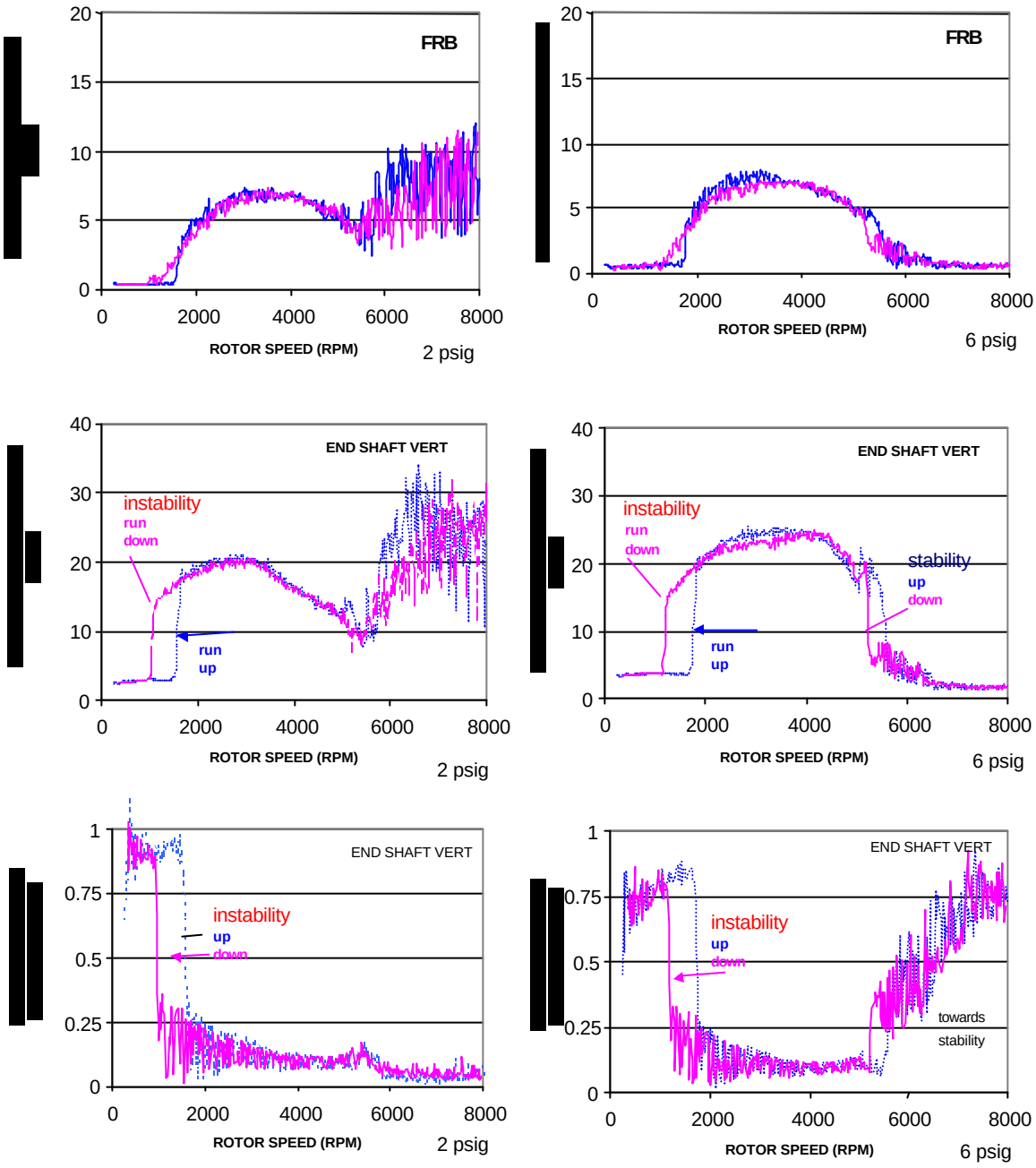

Figure 8. Measured response for rotor-FRB rig. Oil temperature 82F (28 C). Remnant imbalance

Top: Overall p-p motion for floating ring (mils), Middle: Overall p-p motion end shaft vertical (mils), Bottom: ratio of synchronous component to overall motion at shaft end.

LEFT: 13.8 kPa (2 psig), RIGHT: 41.3 kPa (6 psig) feed

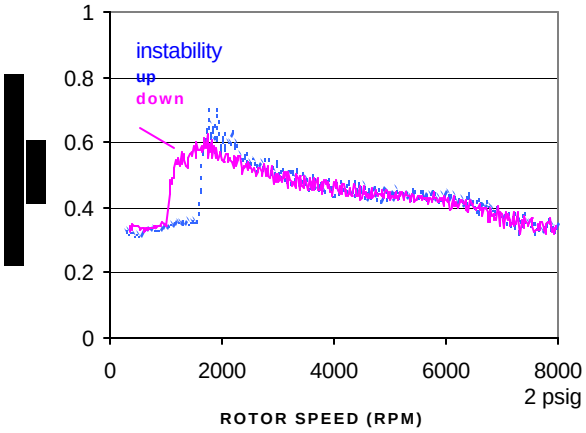

Figure 9. Measured ring speed to rotor speed ratio. Oil temperature 82F (28 C), remnant imbalance, 13.8 kPa (2 psig) feed pressure.

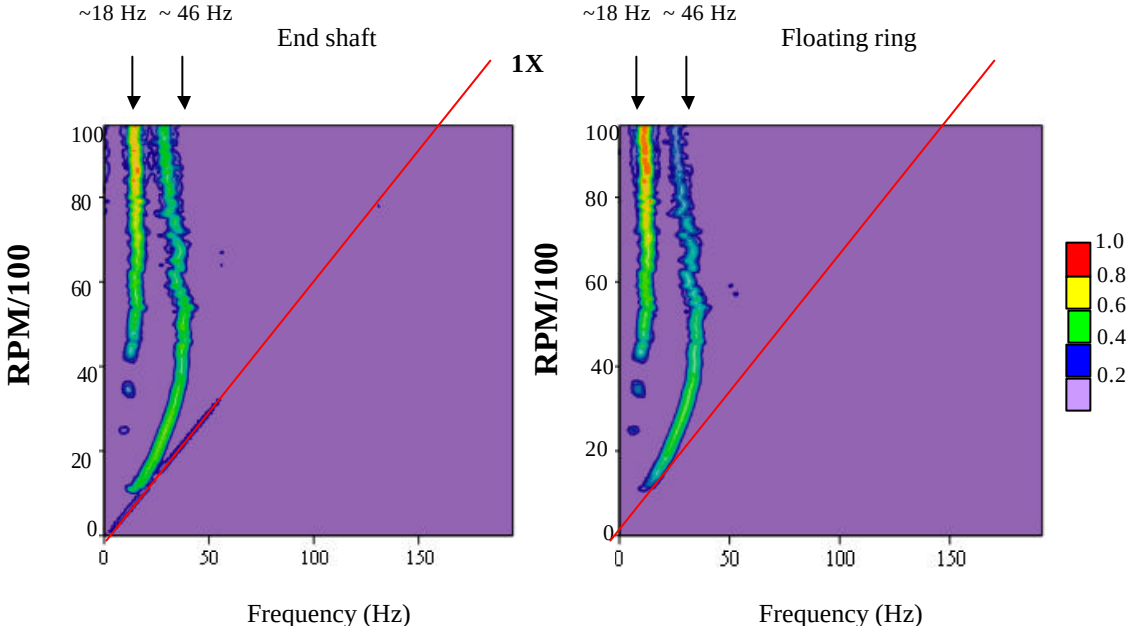

Figure 10 . Contour vibration spectra for measurements with nominal clearance FRB. Feed pressure 13.7 kPa (2 psig) and remnant imbalance.

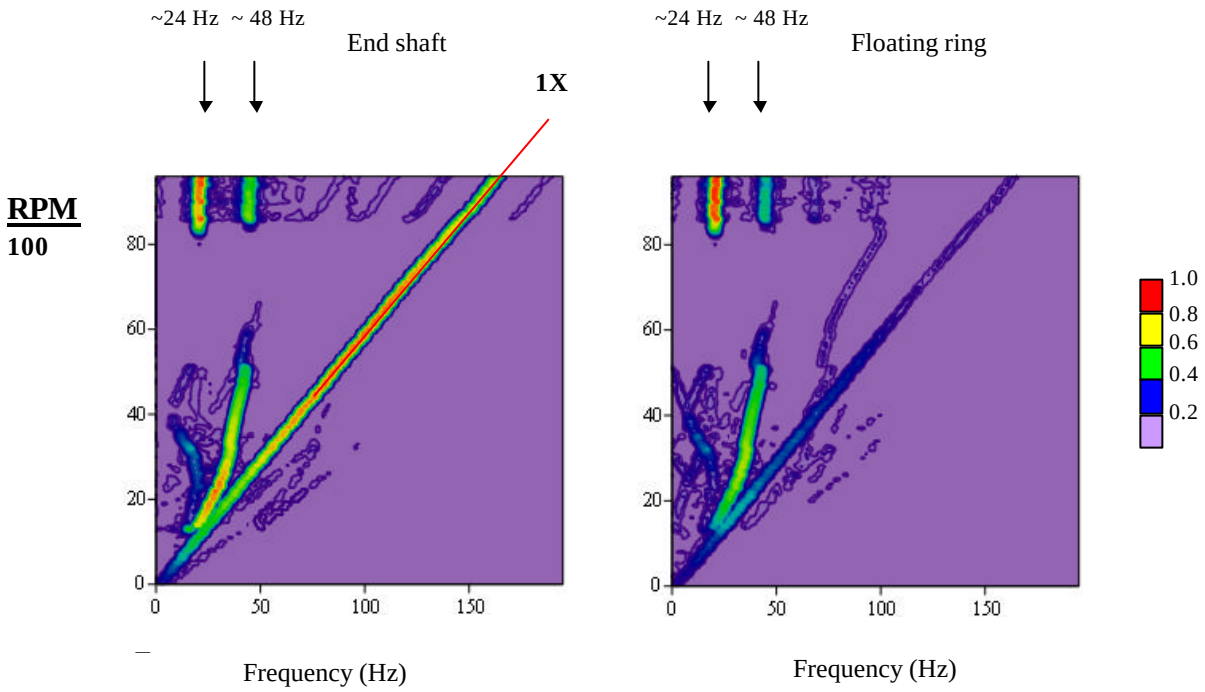

Figure 11. Contour vibration spectra for measurements with nominal clearance FRB. Feed pressure 41.3 kPa (6 psig) and remnant imbalance.

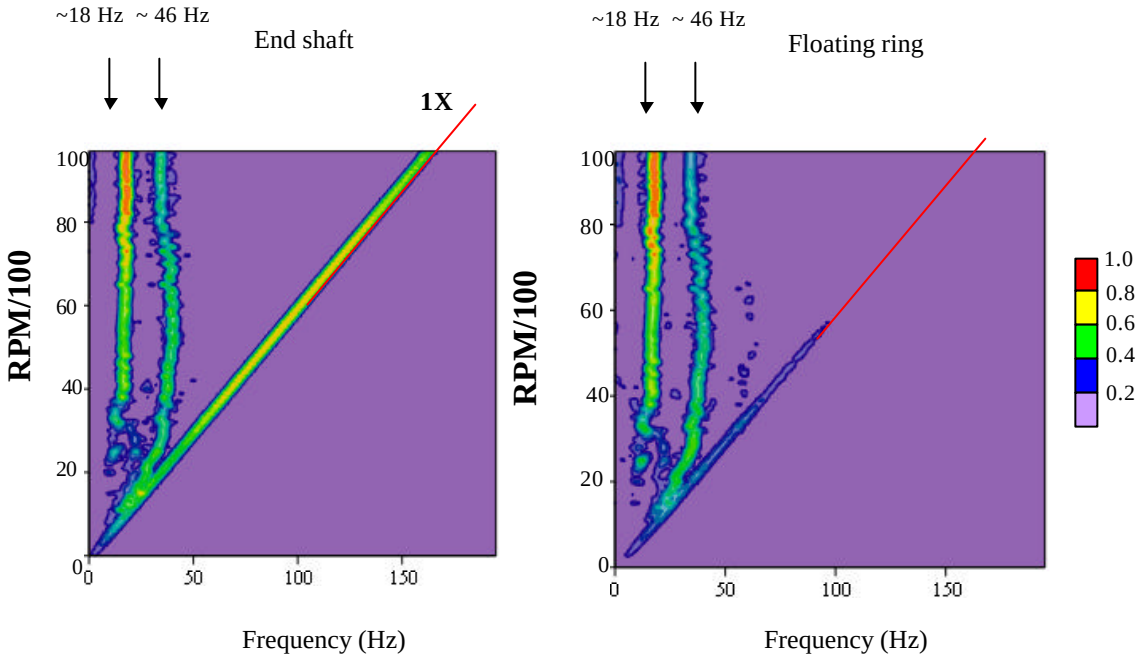

Figure 12 . Contour vibration spectra for measurements with nominal clearance FRB. Feed pressure 13.7 kPa (2 psig) and 6 gram imbalance.

ACKNOWLEDGEMENTS

The support of Honeywell Turbocharging Systems, Inc. and the TAMU Turbomachinery Laboratory are gratefully acknowledged. Thanks to Mr. Sunil Sahay and Gerry LaRue for their interest and insightful recommendations.

REFERENCES

1. Orcutt, F. K. and Ng, C. W., "Steady State and Dynamics Properties of the Floating Journal Bearings," ASME Paper 67-LUB-13, (1967).
2. Shaw, M. and Nussdorfer, T. J., "An Analysis of the Full-Floating Journal Bearing," NACA Report No 866, (1947).
3. Tanaka, M., "A Theoretical Analysis of Stability Characteristics of High Speed Floating Bush Bearings," *Transactions of the Japan Society of Mechanical Engineers*, Vol. 13, N° 61 (1970) 859-863.
4. Tanaka, M. and Hori, Y., "Stability Characteristics of Floating Bush Bearings," ASME *Journal of Lubrication Technology*, Vol. 94, (1972) 248-259.
5. Rhode, S. M. and Ezzat, H.A., "Analysis of Dynamic Loaded Floating-Ring Bearings for Automotive Applications," ASME *Journal of Lubrication Technology*, Vol. 102, (1980) 271-277.
6. Li, C. H. and Rhode, S. M., "On the Steady State and Dynamic Performance Characteristics of Floating Ring Bearings," ASME *Journal of Lubrication Technology*, Vol. 103, (1981) 389-397.
7. Dong, X. and Zhao, Z., "Experimental and Analytical Research on Floating Ring Bearing Engine Applications," ASME *Journal of Tribology*, Vol. 112, (1990) 119-122.
8. Sahay, S. N. and LaRue, G., "Turbocharger Rotordynamic Instability and Control," Proc. 8th Rotordynamic Instability Problems in High-Performance Turbomachinery Workshop, Texas A&M University, TX, (1996) 1-11.
9. Naranjo, J., "Imbalance Response of a Rotor Supported on a Floating Ring Fluid Film Bearing," M.S. Thesis, Texas A&M University, College Station, TX, June (1999).
10. San Andrés, L., "A Test Rig for Measurement of Dynamic Response and Stability of a Rotor Supported on Floating Ring Bearings," *TAMU TRC Report, TRC-B&C-3-97*, College Station, April (1997).
11. San Andrés, L., Modern Lubrication, Class Notes, Texas A&M University, College Station, TX, (2000) (http://metrib.tamu.edu/me626/notes).
12. De Boer, Thomas, "Computational Analysis of Rotors Supported on Floating Ring Journal Bearings," Engineering Thesis, Universiteit Twente, The Netherlands, August (2000).